A coherence-imaging approach to time-resolved charge-exchange recombination spectroscopy in high temperature plasma

J. Howard Plasma Research Laboratory, Australian National University , Canberra, A.C.T., 0200 Australia
L. Carraro, M.E. Puiatti, F. Sattin, P. Scarin, M. Valisa, B. Zaniol, Consorzio RFX, Padova, Italy
R. Konig, J. Chung Max-Planck Institut fur Plasmaphysik, Greifswald, Germany

Summary

We show that a coherence-based, or interferometric approach to spectral analysis of charge-exchange recombination (CXR) emission radiation from high temperature plasma offers some potential advantages over wavelength-domain instruments.

The spectral-line shift and broadening are obtained from measurements of the spectral coherence at a given fixed time delay. This can be monitored using a field-widened electro-optic path-delay-modulated polarization interferometer.

Because the spectral information is encoded at harmonics of the electro-optic modulation frequency, a single detector suffices to capture the spectral information. This opens the possibility for time-resolved two dimensional spectral imaging.

In this paper, we model the performance of coherence imaging systems for realistic measurement scenarios and compare with grating based devices. We especially look at the influence of background and spectral contamination within the measurement passband.

Some new instrument concepts and recent design advances are presented.

Principle of the measurement

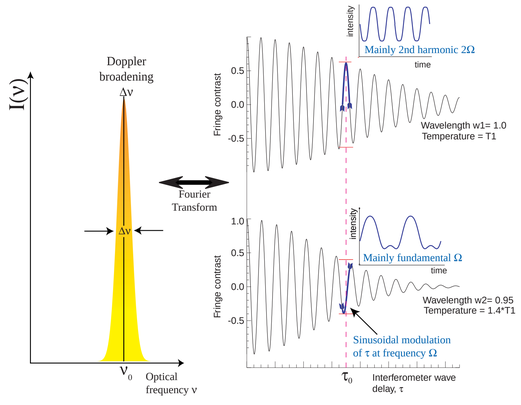

Fig 1. MOSS is a modulated fixed delay Fourier transform spectrometer. The fringe visibiliy (inverse of spectral width) and fringe phase (inverse of line shift) can be monitored by modulating about a fixed delay offset. This generates a time domain interferogram whose harmonic amplitudes convey the light intensity, shift and width.

Coherence imaging (MOSS) camera

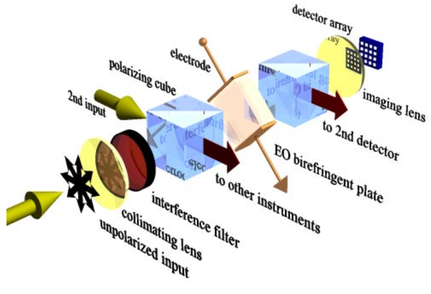

Fig 2. Layout of Modulated Optical Solid (MOSS) spectrometer. The light is collimated by an objective lens before passing through an optical filter to select the spectral line, Following the first poalrizer, the light traverses an electrooptically modulated birefringent LiNbO3 plate (0-100 kHz). Finally the shifted, orthogonal components interfere at the final polarizer, creating an interferogram similar to that shown in Fig. 1.

Why Coherence Imaging Spectroscopy?

Only one detector per spatial channel is required. Allows construction of time-resolved spectroscopic imaging camera. Spectral information is encoded in the temporal frequency domain.

High light throughput. Beacsue there is no slit, the etendue can be orders of magnitude greater than for a grating instrument of comparable resolving power

No instrument function deconvolution

Spread spectrum techniques allow time-resolved high resolution spectroscopy (**SOFT spectrometer**)

Coherence imaging systems are compact and alignment insensitive

Simple Interpretation for Doppler Spectroscopy

Measured signal (interferogram) — 1st moment (phase => flow)

$$I(t) = I_0[1 + \zeta_I\zeta_{plasma}\cos(\phi_0 + \phi_m \sin(\Omega t))]$$

0th moment (intensity) — 2nd moment (contrast => Temperature) — Modulation

$\zeta_I = \exp(-T_I/T_C)$ $\zeta_{plasma} = \exp(-T_S/T_C)$

T_I is the instrument temperature
T_S is the emitting species temperature
T_C is the characteristic temperature set by the instrument delay

Only one "spectral" sampling point required to determine the integrals of intensity weighted temperature and flow.
The full lineshape is required for frequency domain instruments.

Interpreting CX Coherence Images

When unwanted spectral features are passed by the interference filter, the interpretation of the coherence phase and amplitude images can become ambiguous.

By modulating the particle beam source, it is possible using a single-delay modulated interferometer, to characterize the Doppler-broadened CXR emission component against significant pollution from background or nearby spectral features.

BV Model spectrum:

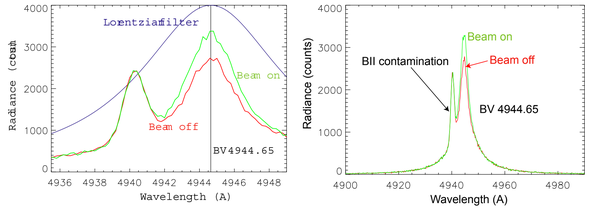

Fig 3. Left: Noise corrupted model spectrum of charge exchange BV emission showing signal enhancement when the neutral beam is on. The model closely matches a typical measured spectrum obtained on the Alcator C-MOD tokamak (Courtesy R. Granetz). Right: The spectrum following application of the narrow bandpass interference filter shown at left.

Extracting the CX component

The coherence camera interferogram measures the sum of all components within the prefilter passband

$$S_p = \sum_i S_i = I_p\left[1 + \zeta_p\cos(\phi_p + \bar{\phi})\right]$$

In the absence of the neutral beam, the interferogram delivers the "complex coherence" of the plasma emission at the preset instrument delay:
$\gamma_p = I_p\zeta_p\exp(i\delta_p)$

I_p is the radiance, ζ_p is the interferogram ontrast and δ_p is the phase shift from the centre-wavelength phase $\phi_0 = 2\pi LB(\nu_0)\nu_0/c$

When the beam is on we obtain the corresponding quantity
$\gamma_b = I_b\zeta_b\exp(i\delta_b)$

The charge exchange contribution can be then recovered

$$\zeta_{cx}\exp(i\phi_{cx}) = \frac{\gamma_b - \gamma_p}{I_b - I_p}$$

and the CX species temperature and flow determined
$\zeta_{cx} = \exp[-T_{cx}/T_C]$
$\delta_{cx} = \kappa\phi_0 v_{cx}$

Statistical modeling

We have generated ensembles of shot-noise corrupted spectra, computed their coherence and applied the above procedure to obtain a statistical estimate for the model temperature of the CX ions. For these simulations, we assume the same light collection efficiencies for both MOSS and grating systems.

Calculated coherence

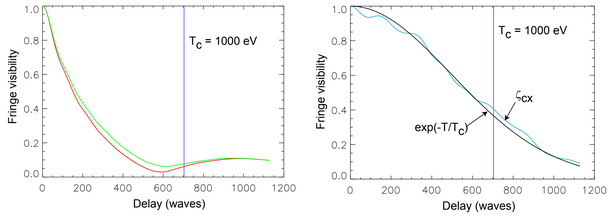

Fig. 4. Left: The fringe visibility versus interferometric phase delay in the beam-off and beam-on cases. The vertical line indicates the delay corresponding to $T_c =1000$ eV.
Right: The extracted noisy, approximately Gaussian, coherence component associated with the beam generated BV radiation. The black curve shows the expected variation for a 1 keV Doppler-broadened emission line..

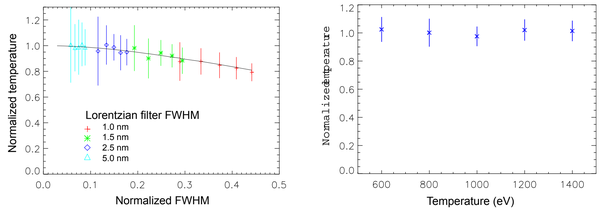

Fig. 5 Results of statistical analysis. Left: The ratio of inferred to true temperature versus normalized Doppler width for a number of bandpass filter widths and temperatures in the range 600-1400 eV. Measurement reliablility decreases for larger filter widths where the fractional modulation of the light intensity produced by the beam is small.
Right: Normalized inferred temperature versus true temperature for wavelength domain instrument.

Fast Framing MOSS Camera

We have constructed a time-resolved coherence-imaging camera for study of 468nm HeII emission from the divertor regions in the W7-AS stellarator.

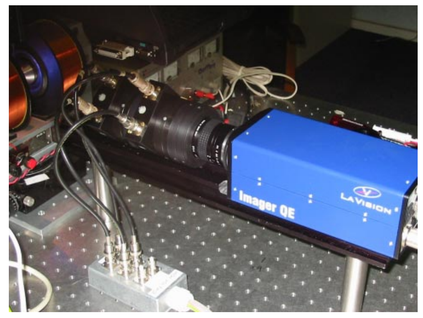

Fig. 6 Photograph of the combined MOSS and fast framing CCD camera designed for 2-d spectral imaging of the divertor regions in the W7-AS stellarator

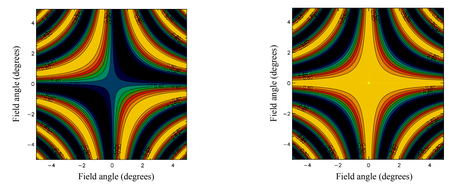

Fig. 7 Left: Interference pattern for single modulator plate of thickness 10mm at 468nm. Centre: The pattern is symmetrized when two plates of thickness 5mm are crossed. Crossing plates compensates thermal drifts. Combining two pairs of crossed plates with intervening half wave plate yields a perfectly flate field.

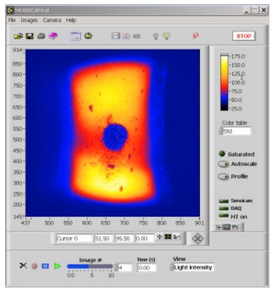

Fig. 8 Front panel of the LabVIEW software designed for control of the Sensicam LE cooled fast framing CCD camera and the MOSS electrooptics. The colour image shows the 468nm emission from a laboratory zinc discharge lamp.

Successive quadrature images of the interferogram are obtained by locking the electrooptic plate modulation with the frame rate of a commercially availablefast-framing CCD camera (PCO Sensicam LE).

The staircase, which is designed to produce phase steps [0, π/2, π, 3π/2] is generated using a custom LabVIEW-based application that both controls a National Instruments PCI-MIO-16-E4 PC-card and communicates with the CCD camera.

Following automatic compensation for the instrument response, sets of four sequential frames can be processed to deliver the interferogram intensity, contrast and phase.